ELSEVIER

Nuclear Instruments and Methods in Physics Research A 431 (1999) 413–427

NUCLEAR INSTRUMENTS & METHODS IN PHYSICS RESEARCH Section A

www.elsevier.nl/locate/nima

The simulation of resistive plate chambers in avalanche mode: charge spectra and efficiency

M. Abbrescia[a,*], A. Colaleo[a], G. Iaselli[a], F. Loddo[a], M. Maggi[a], B. Marangelli[a], S. Natali[a], S. Nuzzo[a], G. Pugliese[a], A. Ranieri[a], F. Romano[a], S. Altieri[b], G. Bruno[b], G. Gianini[b], S.P. Ratti[b], L. Viola[b], P. Vitulo[b]

[a] *Dipartimento Interateneo di Fisica and Sezione INFN, Bari, Italy*
[b] *Dipartimento di Fisica Nucleare e Teorica and Sezione INFN, Pavia, Italy*

Received 26 October 1998; received in revised form 18 March 1999

Abstract

A model to simulate the avalanche formation process and the induced signal in a Resistive Plate Chamber is presented. A first investigation of the effects of various parameters on the performance of this detector is reported. © 1999 Published by Elsevier Science B.V. All rights reserved.

1. Introduction

Resistive Plate Chambers (RPCs) [1] are detectors for ionizing particles presently used in many different experiments performed both with cosmic rays and at accelerators. They will play an important role for the generation of the first level muon trigger in the future experiments CMS and ATLAS at the Large Hadron Collider (LHC).

In these experiments, RPCs will be requested to withstand a large background of neutrons and γ-rays, producing an effective (i.e. taking into account RPC sensitivity) hit rate up to ~ 300 Hz/cm^2 [2]. It is well known that RPCs operated in streamer mode (the way they were originally conceived to work), are unable to handle such high values of incident flux without a global performance degradation (increased inefficiency and power consumption, worse time resolution). The way to overcome these problems lies in operating RPCs in avalanche mode, using lower electric fields and transferring part of the needed amplification from the gas to front-end electronics [3,4].

Since the introduction of this operation mode, a great effort has been made to find out the best conditions concerning gas mixtures, electronics, and detector design parameters (gap width, electrode material, etc.). Despite the huge amount of experimental data collected in various conditions, the understanding of the basic principles of operation of this kind of detector is poor, and a comprehensive theoretical model able to explain and predict the effects of changes of structural parameters on chamber performance is still lacking.

In this paper a Monte Carlo simulation of the avalanche growth and pulse development in RPCs, together with the electronic signal processing, is

* Corresponding author. Tel.: 39-80-5442431; fax: 39-80-5442470.
E-mail address: Marcello.abbrescia@ba.infn.it (M. Abbrescia)

PII: S0168-9002(99)00374-5

presented. This model, based on the Townsend theory of avalanches, represents a first attempt to reproduce the major physical processes taking place in an RPC, and to compute the detector performances, i.e. efficiency, time resolution and charge spectra. This paper is structured as follows: Section 2 explains briefly the model used in the simulation; in Section 3 a detailed study of charge spectra and efficiency, for single gap RPCs, is presented; in Section 4 a similar study is done for double and multi-gap RPCs; Section 5 is devoted to draw some conclusions.

On purpose the comparison between the simulation and the experimental results plays, here, a secondary role. This comparison, in fact, has already been the object of a previous paper [5], where, even if the program used in that occasion was a simplified version of the one available presently, a good agreement between predictions and real data has been shown. Moreover, the examination of the timing performance of RPCs, which is a very basic issue, is not contemplated here because it will be the subject of a forthcoming paper.

2. The model

First, the program considers an ionizing particle which crosses the RPC gas gap generating n_{cl} primary ion–electron clusters. The probability P_{cl} that k clusters are generated in the gap is given by:

$$P_{cl}(n_{cl} = k) = \frac{(g\lambda_{eff})^k}{k!} e^{-g\lambda_{eff}} \tag{1}$$

where $\lambda_{eff} = \dfrac{\lambda}{\cos\phi}$, λ is the primary cluster density (i.e. the number of primary ion–electron clusters generated by the ionizing particle per unit length), ϕ the azimuthal angle of the incident particle $(0 \le \phi < \pi/2)$, and g the gap width. The cluster electrons drift toward the anode and, if the electric field is intense enough, they start avalanching. The probability distribution $P_p^j(x)$ of the initial position x_0^j of the jth cluster (the first cluster is the closest to the cathode) is given by Poisson statistics:

$$P_p^j(x_0^j = x) = \frac{\lambda_{eff}}{(j-1)!}(x\lambda_{eff})^{j-1} e^{-x\lambda_{eff}}, \quad 0 < x < g. \tag{2}$$

Assuming exponential avalanche development, the total charge q at position x is

$$q(x) = \sum_{j=1}^{n_{clust}} q_e n_0^j M_j e^{\eta(x - x_0^j)} \tag{3}$$

where n_0^j is the number of primary electrons of the jth cluster, η the first effective Townsend coefficient (i.e. the Townsend coefficient α minus the attachment coefficient β), and q_e the electron charge (see Fig. 1).

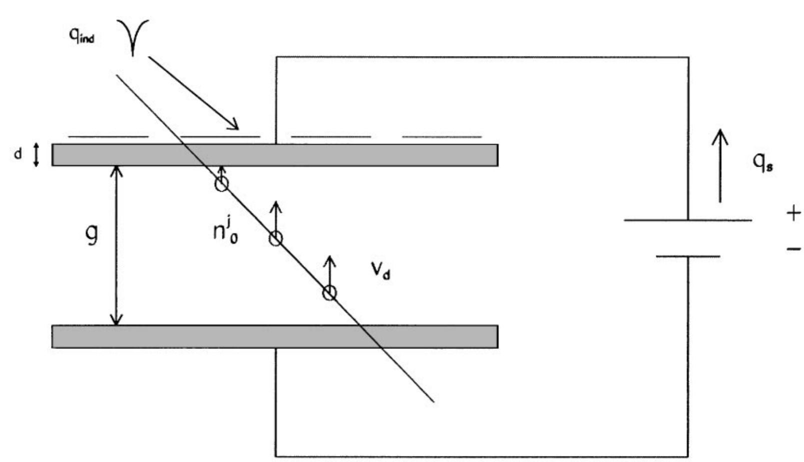

Fig. 1. Signal generation in RPCs.

The factor M_j accounts for the stochastic fluctuations of the exponential growth. In a simplified model [6], valid for low values of the reduced electric field E/p (p gas pressure), the probability that n electrons are produced after a path length $l = g - x_0$ is given by Furry's law:

$$P_F(n_{av} = n) = \frac{1}{N}\exp\left(-\frac{n}{N}\right) \tag{4}$$

where $N = n_0 e^{\eta(g-x_0)}$. Otherwise, for high values of E/p (for what "high values" means, see the detailed discussion in Ref. [6]; however, this is the case of standard operating conditions for RPCs), a Polya distribution must be used:

$$P_P(n_{av} = n) = \left[\frac{n}{N}(1+\theta)\right]^{\theta} \exp\left[-\frac{n}{N}(1+\theta)\right] \tag{5}$$

where the value $\theta = 0.5$ has been chosen [6]. To obtain the factor M in formula (3) a number is taken randomly from Eq. (5) (which has, like formula (3), N as average value) and divided by N.

After simulating the drifting avalanches, the program computes the current i_{ind} induced on the external pick-up electrodes (strip or pads) by the motion of the same avalanches. This is done by means of the Ramo theorem [7], usually expressed with the help of the concept of "weighting field". The read-out electrode has to be put at a "weighting potential" $V_w = 1$, while the others at 0. In these conditions the weighting field $\boldsymbol{E}_w$ (relative to the weighting potential V_w) is computed; note that $\boldsymbol{E}_w$ has the dimensions of an inverse of a length, while V_w is a pure number. For an RPC $\boldsymbol{E}_w$ has a simple expression, being approximately uniform in the gap for pads or strips having dimensions much greater than the gap width. Here, in first approximation, the tail effects on $\boldsymbol{E}_w$ between two adjacent strips have been neglected.

If the bakelite electrode thickness and permittivity are taken into account (the bakelite can be considered as a perfect dielectric, since the avalanche development has a duration < 100 ns, negligible with respect to the material time constant $\rho\varepsilon \sim$ few ms, where ρ and ε are the bakelite resistivity and dielectric permittivity) the weighting potential drop $\Delta V_w = E_w g$ in a gap is given by

$$\Delta V_w = \frac{\varepsilon_r g}{n_g \varepsilon_r g + (n_g + 1)d} \tag{6}$$

where d is the electrode plate thickness, n_g the number of gaps in the detector (in the case of strips placed on one side of the whole RPC), and ε_r the bakelite relative dielectric permittivity. The same result can also be obtained using the generalised Ramo theorem [8], as also shown in Ref. [9].

The current $i_{ind}(t)$ induced by a drifting charge on the external pick-up electrodes, as a function of time (for one cluster) is

$$i_{ind}(t) = -Mq(t)\boldsymbol{v}_d \cdot \boldsymbol{E}_w \tag{7}$$

where $\boldsymbol{v}_d$ is the electron drift velocity in the gas mixture considered. In explicit form (and considering all clusters):

$$i_{ind}(t) = -\boldsymbol{v}_d \cdot \boldsymbol{E}_w q_e e^{\eta v_d \Delta t} \sum_{j=1}^{n_{cl}} n_0^j M_j. \tag{8}$$

Here Δt is the time elapsed from the passage of the ionizing particle in the gap, i.e. from the generation of the primary clusters (which are assumed to be created at the same moment). Formula (8) is useful since, from the simulated current $i_{ind}(t)$, the whole information coming out from an RPC can be reproduced. The simulated signals can drive simulated pre-amplifiers, discriminators, TDCs, ADCs, etc. For instance, in the case of charge sensitive amplifiers, the output voltage (to the discriminators) is simply:

$$v_{out} = P_1 \int i_{ind}(t)\,dt \tag{9}$$

where P_1 is the amplifier charge sensitivity, expressed, for instance, in mV/fC.

If the charge is growing exponentially, then the charge q_{ind} induced on pick-up electrodes can be computed by direct integration of Eq. (8) and is given by

$$q_{ind} = \frac{q_e}{\eta g}\Delta V_w \sum_{j=1}^{n_{cl}} n_0^j M_j [e^{\eta(g-x_0^j)} - 1]. \tag{10}$$

3. Charge spectra and efficiency of single gap RPCs

Simulated spectra of the induced charge q_{ind} for single gap RPCs are shown in Figs. 2 and 3, for three different values of η. The primary ionization density has been chosen to be $\lambda = 5.5\ \mathrm{mm}^{-1}$ (typical of many mixtures currently employed in RPCs), and will be the same throughout this paper, unless otherwise specified. Two cases are considered: a typical "narrow" gap ($g = 2$ mm, Fig. 2) and a "wide" gap ($g = 9$ mm, Fig. 3) RPC. An increase in the value of η has the effect of increasing the average induced charge, as expected from Eq. (10); for instance, in the narrow gap case, $\langle q_{ind} \rangle$ changes from 0.12 pC for $\eta = 8\ \mathrm{mm}^{-1}$ to 2.45 pC for $\eta = 10\ \mathrm{mm}^{-1}$. The corresponding values for $g = 9$ mm are $\langle q_{ind} \rangle = 0.22$ pC for $\eta = 1.5\ \mathrm{mm}^{-1}$ and $\langle q_{ind} \rangle = 2.80$ pC for $\eta = 2\ \mathrm{mm}^{-1}$.

The two set of distributions differ significantly: in the narrow gap case the curves tend to diverge for $q_{ind} \to 0$, while in the wide gap case they tend to vanish. In other words, even if the average induced charge is roughly the same (compare, for instance, the plots corresponding to $\eta = 10\ \mathrm{mm}^{-1}$ and $\eta = 2\ \mathrm{mm}^{-1}$ for the 2 and 9 mm RPCs, respectively), the number of events characterized by small charge is always greater in narrow than in wide gap RPCs; there is also an excess of events in the right tail of the distribution, counterbalanced by less events in the central part (with respect to the 9 mm). The fact that wide gap curves vanish near the origin is almost independent of the value of η; this effect, in fact, is still visible, though barely, also in the distribution corresponding to $g = 9$ mm and $\eta = 1.5\ \mathrm{mm}^{-1}$ of Fig. 3.

Some hints about the basic features of RPCs charge spectra can be obtained by means of analytical calculations, reported in detail in the Appendix. It can be demonstrated that, under some approximations, the distribution of the charge induced by the first cluster (the closest to the cathode, and therefore the one giving rise to most of q_{ind}), is given by

$$P_q(q_{ind} = q) = A q^{\frac{\lambda}{\eta} - 1} \tag{11}$$

where A is an appropriate renormalization constant. This expression states that the charge distribution depends only on the λ/η ratio. The three cases of interest are:

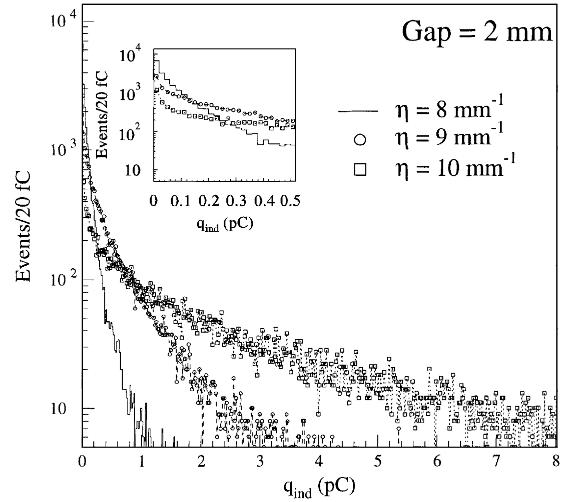

Fig. 2. Simulated spectra of induced charge, for a 2 mm single gap RPC, at different η values; in the small box an enlargement of the region near the origin is reported.

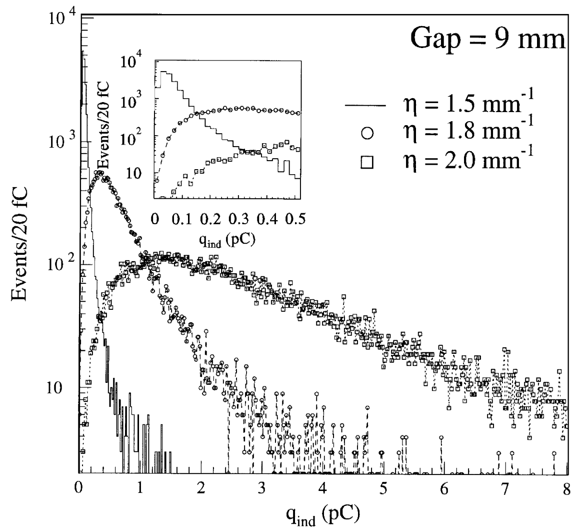

Fig. 3. Simulated spectra of induced charge, for a 9 mm single gap RPC, at different η values; in the small box an enlargement of the region near the origin is reported.

1. $\dfrac{\lambda}{\eta} < 1$; in this case the resulting distribution is strictly decreasing, and diverges for $q \to 0$: this is the typical situation of a narrow gap RPC.

2. $\dfrac{\lambda}{\eta}=1$; in this particular case $P_q(q)=\text{const.}$
3. $\dfrac{\lambda}{\eta}>1$; in this case the resulting distribution is strictly increasing, and starts from 0 for $q=0$: this is typical of a wide gap RPC where, thanks to the large value of gap width g, η can be set conveniently low.

These facts have deep implications for the correct operation of single gap RPCs, in particular from the point of view of the maximum achievable efficiency. In fact, situation (i) is the worst, since both the front-end threshold and the noise level in the chamber have to be drastically reduced. Of course, the events characterized by a charge lower than the experimental threshold (given by electronics or, more likely, by the noise in the chamber) will not be revealed. Therefore a hole will be observed in the region between 0 pC and the threshold, and events with such a low charge will account for the chamber inefficiency. This would suggest to use wide gap RPCs, but the efficiency gain is counter-balanced by the loss in the timing performance of the chamber; this item, however, as already pointed out, is not treated here and will be the subject of a forthcoming paper.

The fact that the ratio λ/η determines the shape of the charge distribution is not surprising: the two processes active in competition in the gap are cluster generation (ruled by $e^{-\lambda x}$, for the first cluster), and avalanche multiplication (ruled by $e^{\eta(g-x)}$). A larger width of active gas is present in wide gaps, and this leads to higher effective efficiency. For instance, in a 2 mm gap, for a given threshold, the useful gas length to produce a visible signal is, roughly, 1.8 mm (depending on η), so that only 200 μm (or much less if η is small) are available to start one ionization process. In wide gaps the useful gas length is a bit larger, since, though operating at smaller η, there are still a few mm left to produce ionizations.

Two main pieces of information can be extracted from RPC charge distributions. The first is the fraction of events with clusters characterized by an "avalanche gain" G_{av} greater than a given value; G_{av} is defined as the ratio between the actual charge $q_j(g)$ arriving at the anode and the charge of primary electrons in the cluster $G^j_{av}=\dfrac{q_j(g)}{q_e n^j_0}$. If the gain of at least one avalanche exceeds $e^{20}\sim 4.85\times 10^8$, than this event is referred to as a "streamer". Even if streamer formation is very complex and depends also on the gas mixture, the number of these events can give a rough estimate of streamer probability, useful mainly to make relative comparisons. An absolute comparison with the experimental data should take into account the fact that streamer formation is strongly affected by the space charge in the detector, whose simulation requires more detailed calculations.

The second information is efficiency; this, in the case of charge sensitive front-end amplifiers, can be computed as

$$\varepsilon(q_{thr}) = 1-\int_0^{q_{thr}} P_q(q_{ind})\,dq_{ind} \tag{12}$$

i.e. by counting the fraction of events characterized by a charge greater than a certain electronic threshold q_{thr}; in this paper, q_{thr} has been fixed to 80 fC, which means that front-end electronics should be sensitive to charges greater than 40 fC (only one half of the induced charge reaches the electronics, due to the strip termination on both sides). 40 fC is typical of the present detector layout, and is set, mainly, by pick-up noise.

The efficiency and streamer fraction, computed in the two cases $g=2$ and $g=9$ mm as outlined above, are reported as a function of η in Fig. 4. The 9 mm RPC curves are markedly steeper than the 2 mm ones, i.e. the transition from low to high efficiency or streamer probability takes place more suddenly. This is due to the fact that avalanche processes depend, roughly, on the "chamber gain factor" $G_{ch}=\eta g$; when g is large, a small absolute variation in η means a large change in G_{ch}. Once fixed the detector efficiency, wide gap RPCs are characterized by a much lower streamer probability with respect to narrow gap RPCs. This is evident from Fig. 4, where the width of the operating plateau, i.e. the region where the efficiency is reasonably high ($>90\%$), and the streamer probability is low ($<10\%$), can also be inferred. For the 2 mm this region practically does not exist, while for the

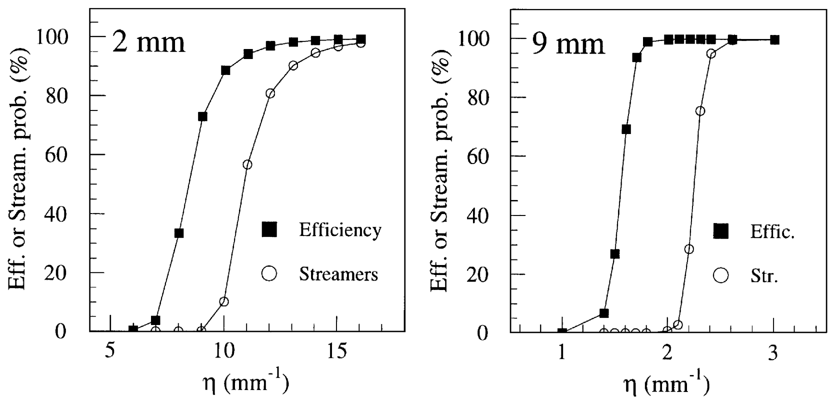

Fig. 4. Efficiency and streamer fraction in single 2 and 9 mm gap RPCs, versus the first effective Townsend coefficient.

9 mm it is about $\Delta\eta = 0.6\ \mathrm{mm}^{-1}$ wide; the operating plateau, in this approximation, increases as the gap increases. There is another equivalent way to see the same effect; at 90% efficiency, the streamer contamination in a 1 mm gap is about 75 %, which decreases to $\sim 20\%$ and to $\sim 0.1\%$ for 2 and 3 mm, respectively. The streamer fraction for gap widths greater than 4 mm is negligible even at $\varepsilon = 95\%$.

Obviously, streamer events are localised toward the right tail of charge spectra; in Fig. 5 the charge distribution corresponding to $g = 2$ mm and $\eta = 10\ \mathrm{mm}^{-1}$, with the streamer events evidenced, is shown again. The fact that not all the events characterized by $q_{\mathrm{ind}} > 2.7$ pC are streamers, is due to the different number of electrons contained in the primary clusters.

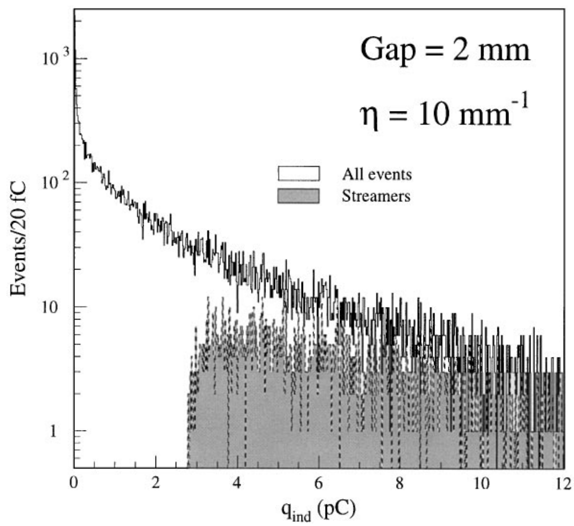

Fig. 5. Simulated induced charge spectra, for a single 2 mm RPC, with streamer events evidenced.

3.1. Variations in the primary ionization density

In addition to η and g, another important parameter, namely, the gas mixture composition, affects RPC operation. Different gas mixtures are, in general, characterized by different values of the primary ionization density; this, in turn, is closely related to the charge spectra shape. λ, for the gas mixtures usually employed, is generally contained between 2 and 8 mm^{-1}. Lower values of λ cannot be used because they would give rise to high intrinsic inefficiency, due to a lack of primary pairs (this inefficiency is just given by $e^{-\lambda g}$). Higher values are not common for the gas usually employed in RPCs or similar detectors. In the following, three items will be examined: the effect of changes in the value of λ on charge spectra, on streamer probability, and the effect of different angles for incident particles on the chamber.

Simulated q_{ind} spectra for a single gap 3 mm RPC are reported in Fig. 6; here λ varies from 4 to 8 mm^{-1}, while $\eta = 6\ \mathrm{mm}^{-1}$. Since the charge distribution depends, roughly, on the ratio λ/η, and in this case λ/η passes from a value smaller to a value greater than 1, the different shapes of charge

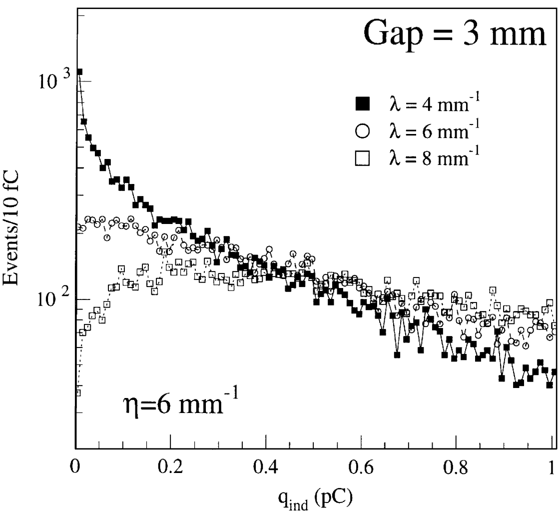

Fig. 6. Charge spectra of a 3 mm single gap RPC, for different values of the primary ionization density.

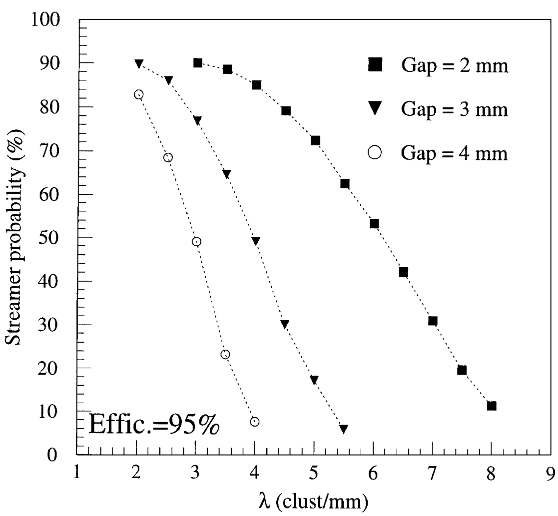

Fig. 7. Streamer probability, as a function of the primary ionization density, for different values of the gap width.

spectra, already evidenced before, are present. Since the number of primary clusters increases linearly with λ so the induced charge does, and therefore $\langle q_{\mathrm{ind}} \rangle$ passes from 0.71 pC ($\lambda = 4\ \mathrm{mm}^{-1}$) to 1.44 pC ($\lambda = 8\ \mathrm{mm}^{-1}$). The corresponding streamer probability changes from 0.20% to only 0.35%, respectively. In fact, gas mixtures characterized by high λ allow an operation mode less contaminated by streamers.

In Fig. 7 the streamer fraction is reported as a function of λ for different values of the gap width; the curves are obtained at constant detector efficiency (95%). In the 2 mm case, an increase of λ from 4 to 7 mm^{-1} decreases the streamer probability from about 85 to 25%; similar behaviours are present for the other values of the gap width. This effect has been already experimentally verified by comparing the performance of RPCs filled with Ar/isobutane or Freon based gas mixtures [10].

A change in the incidence angle of an ionizing particle has, in first approximation, the same effect of a change in the value of λ, according to the rule $\lambda_{\mathrm{eff}} = \lambda/\cos\phi$. When $\phi \neq 0$, the number of primary clusters generated is greater than in the case of perpendicular tracks, and this has the effect of increasing the average value of q_{ind}. Moreover, as already pointed out, the charge distribution is more "detached" from the origin (since η is constant and λ_{eff} is increasing), which allows to reach full efficiency, both in avalanche and streamer mode, at lower operating voltages. The efficiency and streamer probability curves, for a single gap 3 mm RPC, in the case of particles crossing the chamber perpendicularly or with angles $\phi = 45^0$ and $\phi = 60^0$ are reported in Fig. 8. If, on the same chamber, particles with different crossing angles are impinging, the overall effect is to slightly narrow the operating plateau. This is due to the fact that the detector has to be fully efficient for particles crossing the RPCs perpendicularly, and generating less primary clusters; thus the left margin of the operating plateau in Fig. 8 is determined by the efficiency curve for $\phi = 0^0$. The streamer probability, on the contrary, is mainly due to events with a large crossing angle and more primary clusters; the right margin of the operating plateau, therefore, is determined by the streamer probability curve for $\phi = 60^0$. In Fig. 8 the operating plateau is reduced from $\Delta\eta = 0.45$ to $0.31\mathrm{mm}^{-1}$.

3.2. Variations in the model of statistical fluctuations

Finally, it is interesting to study the effect of avalanche fluctuations on the shape of charge

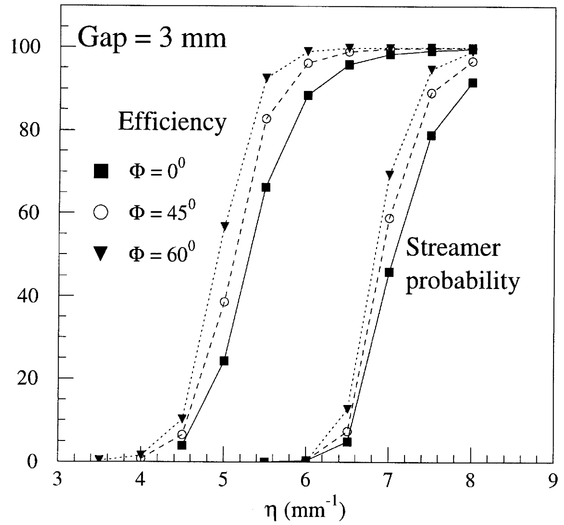

Fig. 8. Efficiency and streamer probability in single 3 mm gap RPCs, for incidence angles $\phi = 0°$, $\phi = 45°$ and $\phi = 60°$.

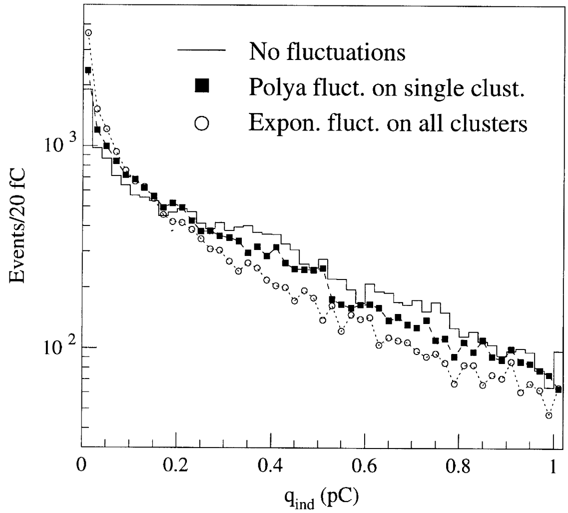

Fig. 9. Induced charge spectra for different types of statistic avalanche fluctuations.

spectra. These fluctuations are just statistical in origin and are not related to a change in the number of primaries, their position, or to the cluster size; they are closely connected to the stochastic nature of avalanche multiplication (see, for a detailed description, Ref. [6]). Different models, based on slightly different theoretical considerations, may be employed for these fluctuations. The charge spectrum in the ideal case of no statistical fluctuations, for a 2 mm single gap RPC at $\eta = 9\ \mathrm{mm}^{-1}$, is reported in Fig. 9; in addition, charge spectra obtained in the approximation used in this paper (Polya-type fluctuations applied separately on each avalanche), and the approximation used by other authors [11] (exponential fluctuations on the sum of all avalanches) are reported in the same figure. One of the effects of avalanche fluctuation is to move the charge spectra toward the y-axis (leaving constant the average charge $\langle q_{\mathrm{ind}} \rangle$), giving rise to an increased chamber inefficiency. This is much more marked in the case of exponential fluctuations with respect to Polya, due to the shape of the two weighting functions used. In this case the inefficiency, in fact, changes from 22.3% (no fluctuations), to 26.9% and 36.4% (Polya-type and exponential fluctuations, respectively). The available experimental results do not allow to discriminate between these two options, since, in the region close to the y-axis, measures of q_{ind} are greatly affected by the noise in the chambers, and due to the uncertainty about the value of η at a given operating voltage. However, the fact that experimental single gap RPC efficiency reaches almost 100% without high streamer contamination, might suggest that the right model could be the Polya-type; this is also favoured by theoretical considerations.

4. Charge spectra and efficiency for double and multi-gap RPCs

Simple layouts of single, double and multi-gap RPCs are shown in Fig. 10. In single and multigaps the strips are on one side of the whole detector while the ground plate is on the other side. In a double gap the strips are in the middle of the two gaps, and the ground plates on the external sides. In this way the sum of the signals coming from the two gaps is obtained on the strips placed in between. This has deep implications on the signal read-out by pick-up strips. From Fig. 10, where the read-out strips are evidenced, and from the discussion

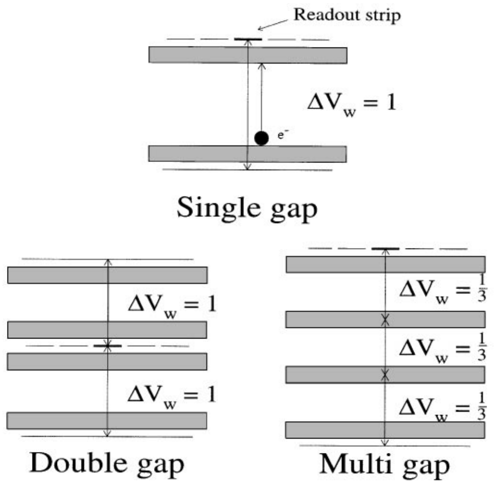

Fig. 10. Simple layouts of single, double and multi-gap RPCs, for the Ramo theorem.

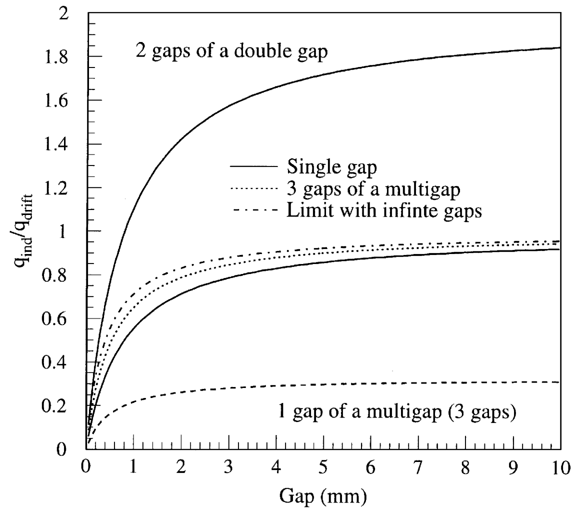

Fig. 11. Ratio between total induced charge and drifting charge per gap in single, double and multigap RPCs.

reported in Section 2 (Eq. (6)), it can be deduced that in a single gap the weighting voltage drop is $\Delta V_w \sim 1$. In a double gap, $\Delta V_w \sim 1$ per gap, while in a multi-gap (with three gaps) $\Delta V_w \sim 1/3$ per gap. This means that, once fixed the charge per gap which is drifting inside the detector, the charge per gap induced on the external pick-up strips is about a factor 3 lower in the multi-gap case, with

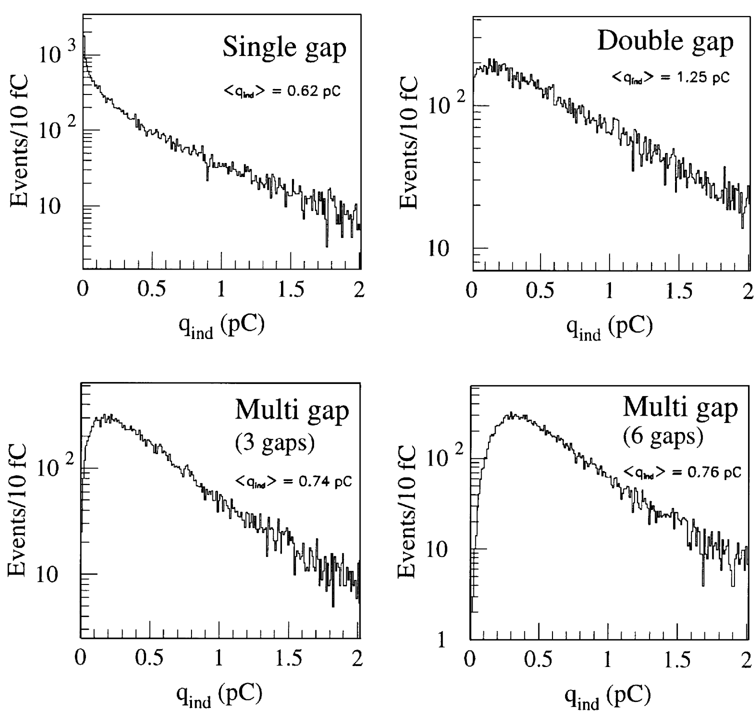

Fig. 12. Simulated charge spectra for 2 mm single, double and multi-gap RPCs, at $\eta = 9$ mm^{-1}.

respect to single and double gaps. Note that there is a difference between the double gap model usually employed (and shown in Fig. 10) and a multi-gap with just two gaps; a factor of 2 in the induced charge derives from this small configuration difference.

There is a simple way to look at the effects of this phenomenon. Consider an RPC where, for instance, a charge $q_{\mathrm{drift}} = 1$ pC is drifting in each gap. The ratio between q_{ind} (the total charge induced by all the gaps) and q_{drift}, which is directly related to the factor ΔV_{w} computed in Section 2, is reported in Fig. 11, for different detector configurations and versus the gap width. In a single 2 mm gap RPC, with bakelite electrodes 2 mm thick, $\frac{q_{\mathrm{ind}}}{q_{\mathrm{drift}}} \sim 0.7$, in a double gap $\frac{q_{\mathrm{ind}}}{q_{\mathrm{drift}}} \sim 1.4$, in a multi-gap (of 3 gaps) about $\frac{q_{\mathrm{ind}}}{q_{\mathrm{drift}}} \sim 0.8$. In Fig. 11 also the ideal case of a multi-gap with an infinite number of gaps is reported (i.e. the $\lim_{n_g \to \infty} \Delta V_{\mathrm{w}}$); an increase in the number of gaps beyond 3 has practically no effect on the induced charge that can be read-out on the external electrodes.

The conclusion that can be drawn is that, apparently, either a higher electronic threshold can be used in the double gap case (with respect to single and multi-gap), or the same threshold can be used and the double gap RPCs can be operated with a drifting charge about a factor 2 smaller. Obviously, lower drifting charge per gap q_{drift} means, for instance, higher rate capability.

However, there is another effect which takes place going from single to double and multi-gaps,

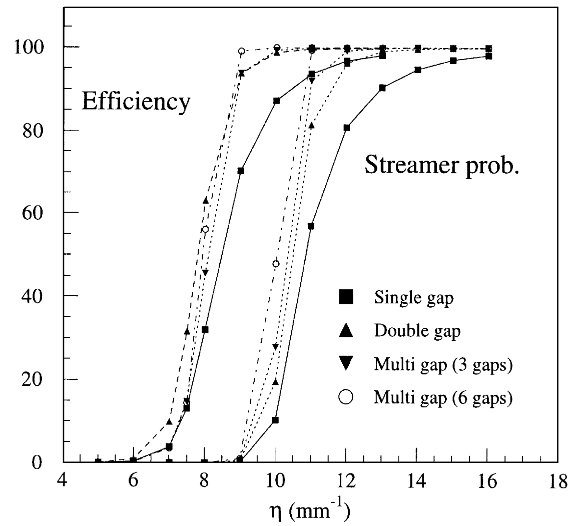

Fig. 14. Efficiency and streamer probability for single, double and multi 2 mm gap RPCs.

which compensates the disadvantage of a lower ΔV_{w} for multi-gap. The point is that, again, the charge spectra shape changes. This is just a statistical effect, due to the fact that double and multi-gap spectra are the convolutions of two or more single gap spectra. The comparison among the q_{ind} charge distributions for four types of RPCs is reported in Fig. 12: RPCs made of 2 mm gaps, in single, double and in the multi-gap (3 or 6 gaps) configurations; in the four cases $\eta = 9\ \mathrm{mm}^{-1}$. The small correlations,

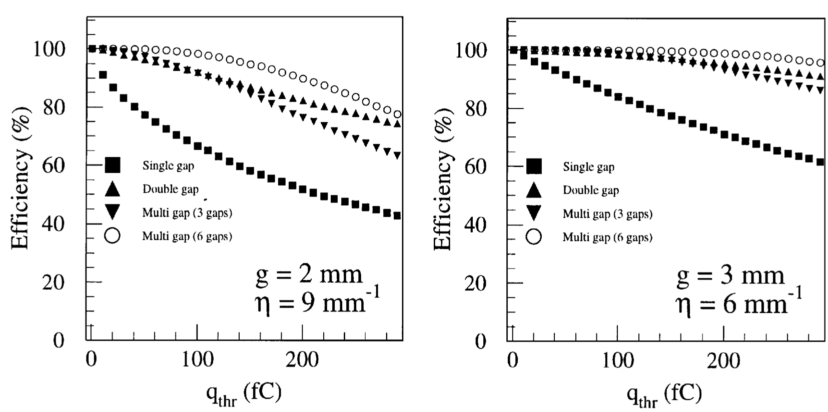

Fig. 13. Efficiency versus electronic threshold for single, double and multi gap 2 and 3 mm RPCs.

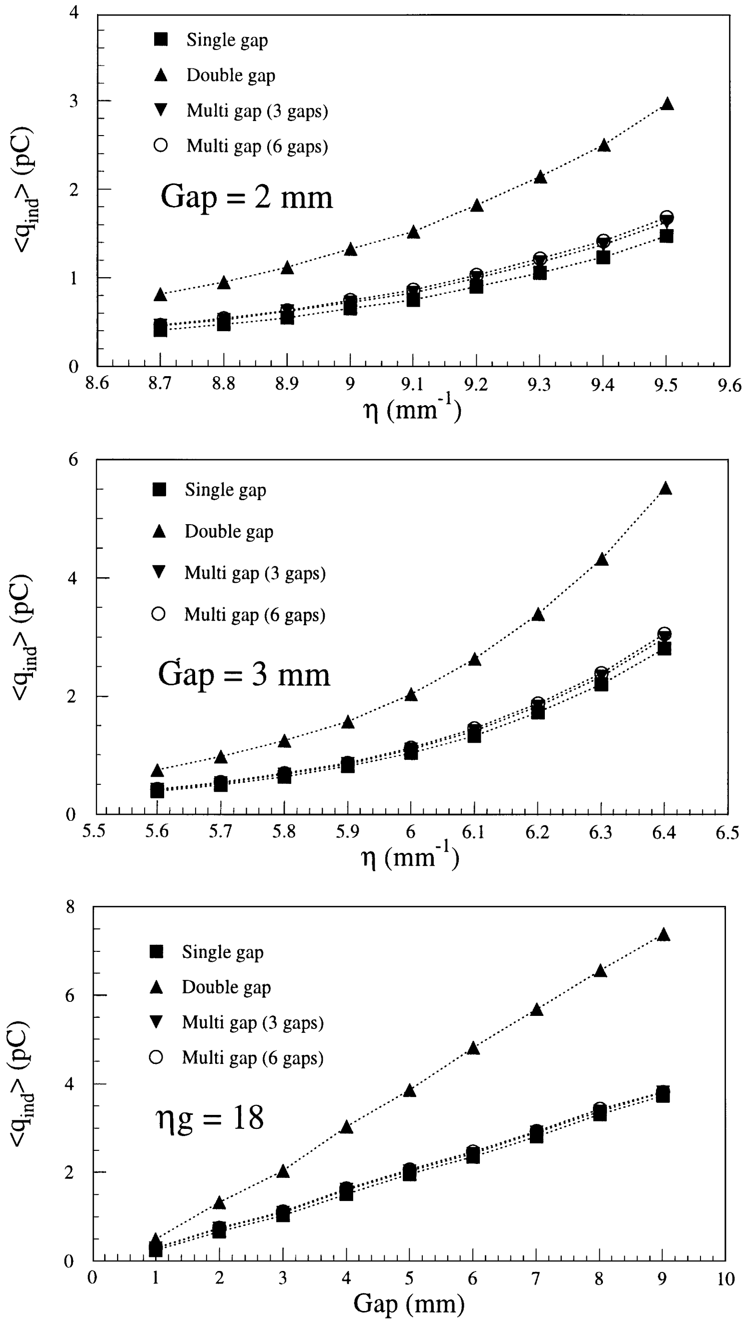

Fig. 15. Average induced charge for single, double and multi-gap 2 and 3 mm RPCs.

if any, that can arise from leaving, in multi-gaps, the central electrodes floating, are, here, neglected. Single gap spectrum exhibits a monotonically decreasing shape; the double and the multi-gap, a sort of "Landau" shape, with a well defined peak detached from the origin and a long tail toward the right. Even if the multi-gap spectrum $\langle q_{\text{ind}} \rangle$ is roughly half than that of the double gap, the distribution is more detached from the origin, and this effect is more and more evident as the number of gaps increases.

As already pointed out, the achievable efficiency depends strongly on the charge spectrum behaviour near the origin. The efficiency, versus the value of the electronic threshold q_{thr}, for 2 and 3 mm single, double and multi-gap RPCs (η has been fixed to typical operation values, i.e. 9 and 6 mm^{-1}, respectively) is reported in Fig. 13. The region of interest is typically between 0 and 200 fC (corresponding, in the case of strip read-out, to 100 fC to the charge pre-amplifiers), where the performance of double and multi-gaps is essentially the same, while single gap RPCs seem to be disadvantaged.

The great improvement achieved when passing from a single gap to a double or multi-gap configuration lies in the fact that, even with small gap widths (≤ 3 mm) it is possible to operate a fully efficient detector with a very low streamer contamination. Efficiency (for $q_{\text{thr}} = 80$ fC) and streamer fraction versus η are shown in Fig. 14, again for the four cases already considered. Pairs of curves (efficiency and streamer fraction for the different configurations) are roughly parallel to each other; however the slopes of these curves increase as the number of gaps increases. The overall effect is to widen the chamber operating plateau. Again, the behaviour of double and multi-gap RPCs is essentially the same, and an increase in the number of gaps from 3 to 6 practically has no advantage.

The average value of the charge q_{ind} induced on pick-up electrodes, for single, double and multi-gap (3 gaps) RPCs, is shown in Fig. 15. In Fig. 15a and b the gap width is fixed, at 2 or 3 mm, and η (that means the operating voltage) is changed. $\langle q_{\text{ind}} \rangle$ in the case of double gap is about twice that of single and multi-gaps, as already explained. As expected by (10), at increasing operating voltage, $\langle q_{\text{ind}} \rangle$ increases roughly exponentially. In Fig. 15c the gap width is changed, keeping constant and equal to 18 the "chamber gain factor" $G_{\text{ch}} = \eta g$. In this case $\langle q_{\text{ind}} \rangle$ increases roughly linearly as the gap increases; this means that, to obtain the same operating regime with wider gap RPCs, G_{ch} should decrease. This is equivalent to say that the electric field employed has to be lower and lower as the gap width increases, an effect already clearly verified experimentally several times. The fact that, at constant ηg, the average induced charge increases with the gap width is not surprising. This is due to two effects: the first is the fact that the number of primary clusters depends linearly on the gap width. The latter is that the first cluster (the one giving rise to most of the induced charge) is created at an average distance $1/\lambda$ from the cathode. The "effective gap" available for multiplication, therefore, is $g - 1/\lambda$. If the chamber gain factor is kept constant, i.e. $G_{\text{ch}} = \eta g = K$, then the "effective" multiplication factor is

$$\eta\left(g - \frac{1}{\lambda}\right) = \frac{K}{g}\left(g - \frac{1}{\lambda}\right) = K - \frac{K}{g\lambda} \tag{13}$$

which increases as the gap increases.

5. Conclusions

A model describing the basic processes taking place in Resistive Plate Chambers operated in avalanche mode has been developed. The model has been used to reproduce the available experimental data, and explains quite well most results, obtained in many operating conditions and with many kinds of chambers (single, double and multi-gaps) [5]. The agreement between the simulation and real data is good.

The model can be used to choose among different RPC types, depending on the required performance; for instance:

1. wide gap RPCs could be better than narrow gaps for what concerns efficiency; the opposite is true for what concerns time resolution;
2. multi-gap RPCs do not show any significant improvement with respect to double gap RPCs.

Obviously, the simulation can be improved. It would be easy to write down a list of physical effects that have not been included, because they are negligible in first approximation or just too difficult to be taken into account. Therefore a few considerations about the validity range of this simulation are in order. In the present state, the simulation does not include any space-charge effect, and so only RPCs operated in the so-called "pure avalanche mode" are correctly described.

Single gap RPCs can be assumed to operate in pure avalanche mode up to the knee of their efficiency plateau. This means that the simulation can predict:

1. position and slope of the efficiency curves up to $\sim 90\%$;
2. charge spectra up to the operating voltage corresponding to this efficiency value;
3. time properties (time resolution and time walk); this can be done for operating voltages greater than the ones considered in the preceding points, since timing is given by the crossing of an electronic threshold, which takes place in the early stage of avalanche development, when space-charge effects are negligible.

For double and multi-gap RPCs, where each gap can be operated at lower gain, these limits are pessimistic (in particular the one regarding efficiency). Beyond these limits corrections must be applied, anyway.

At the moment a great effort is being made to include in the model some of the missing effects. For instance, there is some experimental evidence that space-charge effects could be responsible for a change in the charge spectra shapes (for high values of q_{ind}), as the operating voltage is increased beyond the values characteristic of the "pure avalanche" mode [11–15]. To take into account this effect, a more refined calculation of the effective electric field (i.e. the external field plus the field generated by the electrons and the ions of the avalanches) is needed and is in progress [16,17].

Other important items have already been included, even if the corresponding results have not been reported here; this is the case of the effects due to possible deformations in the gas gap or due to the spacers. Another, easy in principle to include but difficult from a computational point of view, is the prediction of the number of strips fired per event, i.e. the strip multiplicity.

However, by far the most interesting of these problems, at the moment only partially investigated, is the simulation of the dynamical behaviour of RPCs, when the flux of incident particles is not negligible. In this situation a delicate balance between the process of electrode discharge (due to the electron avalanche collection) and charging-up (thanks to the external power supply) is present. In this case some parameters which have not been considered here, like resistivity, play a fundamental role; the effect of resistivity on the rate capability is currently under study. This is, in fact, a primary issue for the future, since, at LHC, RPCs will operate in a high background environment and, in general, a high detection rate will be required.

Appendix. Analytical charge spectra computation

As already pointed out in the text, a first insight about the charge spectra shapes in RPCs can be obtained by means of simple analytical calculations; although, differently from the full Monte-Carlo simulation, certain approximations must be done, this task is very instructive, because highlights important general features of RPC behaviour.

Neglect the fluctuations in the number of electrons n_0^j contained in each cluster and in the gas gain, assuming both to be constant and equal to their average values. In this case, the charge q_{ind} induced by the drift of the jth cluster toward the anode is an analytical function of the initial cluster position x_0^j. Associated with x_0^j there is its probability distribution function (p.d.f.) $P_p^j(x)$, so the problem is reduced to compute the p.d.f. of an analytical function of another p.d.f. This can be done applying directly the results of probability theory (see, for instance, [18]). The result is that the p.d.f. $P^j_{q_{\mathrm{ind}}}(y)$ of the q_{ind} induced by the jth cluster is given by

$$P^j_{q_{\mathrm{ind}}}(y) = R_j \frac{B^{-\frac{\lambda}{\eta}}}{(j-1)!}\left(\frac{\lambda}{\eta}\right)^j \left|\log\left(\frac{y}{B}\right)\right|^{j-1} y^{(\frac{\lambda}{\eta}-1)}$$

$$= R'_j \left|\log\left(\frac{y}{B}\right)\right|^{j-1} y^{(\frac{\lambda}{\eta}-1)} \qquad (14)$$

where

$$B = \frac{q_{\mathrm{e}} M n_0 \Delta V_{\mathrm{w}}}{\eta g} \mathrm{e}^{\eta g}$$

and R_j and $R'_j = R_j \frac{B^{-\frac{\lambda}{\eta}}}{(j-1)!}\frac{\lambda j}{\eta}$ are appropriate renormalization constants.

This distribution is valid up to $q_{\mathrm{ind}}(\mathrm{max}) = \frac{q_e}{\eta g} n_0 M \Delta V_{\mathrm{w}}(\exp \eta g - 1)$, the maximum achievable value for q_{ind}. In the case of $j = 1$ (the cluster generated closest to the cathode, which gives rise to most of the induced charge) the above formula reduces to

$$P^{j=1}_{q_{\mathrm{ind}}}(y) = R_1 \frac{\lambda}{\eta} B^{-\frac{\lambda}{\eta}} y^{(\frac{\lambda}{\eta}-1)} \sim R'_1 y^{(\frac{\lambda}{\eta}-1)} \tag{15}$$

where in the last expression the renormalization constant has absorbed all not-interesting factors, which are constant for a given operating voltage and gas used.

The average charge induced by the first cluster can be computed as the mean of formula (15):

$$\langle q_{\mathrm{ind},j=1} \rangle = \frac{\frac{\lambda}{\eta}}{\frac{\lambda}{\eta}+1} q_{\mathrm{ind}}(\mathrm{max})$$

$$= \frac{\frac{\lambda}{\eta}}{\frac{\lambda}{\eta}+1} \frac{q_e}{\eta g} n_0 M \Delta V_{\mathrm{w}} (e^{\eta g} - 1). \tag{16}$$

This expression (and similar for the other clusters) was already derived in a different way [9].

For the charge induced by the second and third clusters, the following expressions result:

$$P^{j=2}_{q_{\mathrm{ind}}}(y) = -R_2 \left(\frac{\lambda}{\eta}\right)^2 \log \frac{y}{B} B^{-\frac{\lambda}{\eta}} y^{(\frac{\lambda}{\eta}-1)}$$

$$\sim R'_2 \log y y^{(\frac{\lambda}{\eta}-1)} \tag{17}$$

$$P^{j=3}_{q_{\mathrm{ind}}}(y) \sim R_3 \frac{1}{2} \left(\frac{\lambda}{\eta}\right)^3 \left(\log \frac{y}{B}\right)^2 y^{(\frac{\lambda}{\eta}-1)}. \tag{18}$$

The p.d.f. of q_{ind} computed above are reported in Fig. 16, superimposed to the distribution obtained by a reduced version of the Monte Carlo, where the same approximations made in the analytical calculations have been done. Two cases are considered: a 2 mm ($\eta = 9\ \mathrm{mm}^{-1}$), and a 9 mm single gap RPC ($\eta = 2\ \mathrm{mm}^{-1}$). The difference between the case of $\lambda/\eta > 1$ and $\lambda/\eta < 1$ is evident. The 9 mm spectrum is characterized by a higher maximum value of the induced charge; this is due to the large value of the factor ΔV_{w} in a wide gap.

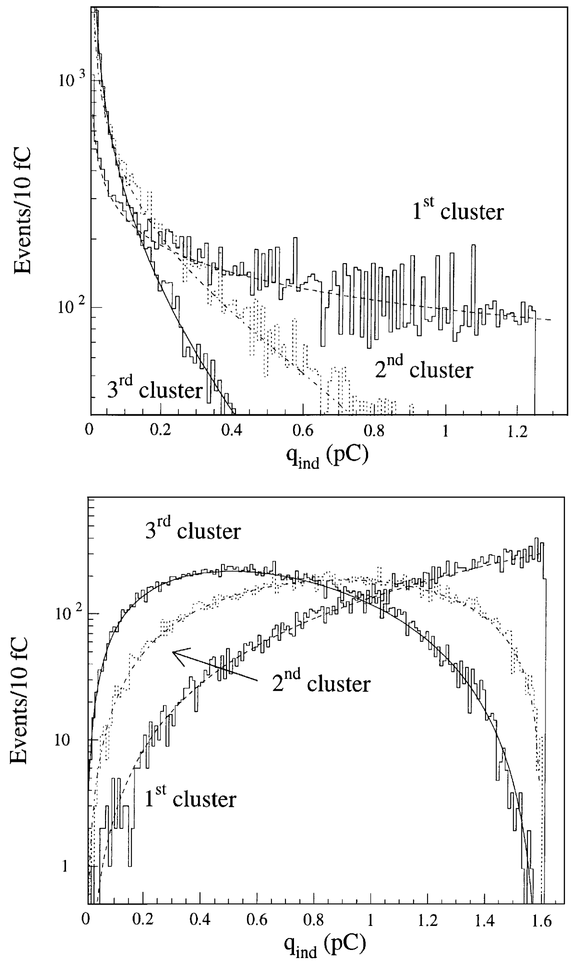

Fig. 16. Simulated induced charge spectra, for single 2 and 9 mm gap RPCs, taking into account only the contribution from the first, the second or the third cluster.

The charge distribution due to the contribution of all clusters is the convolution of $P^{j=1}_{q_{\mathrm{ind}}}(y)$, $P^{j=2}_{q_{\mathrm{ind}}}(y)$ etc.; the related integral, however, is not analytically solvable, so the distribution must be derived by means of numerical methods.

References

[1] R. Santonico et al., Nucl. Instr. and Meth. 187 (1981) 377.
[2] The RPC project, from the Muon Technical Design Report, CERN/LHCC 97-32, CMS TDR3, 15 December 1997.

[3] R. Cardarelli et al., Nucl. Instr. and Meth. A 333 (1993) 399.
[4] I. Crotty et al., Nucl. Instr. and Meth. A 337 (1994) 370.
[5] M. Abbrescia, et al., Talk presented at the 7th Meeting on advanced detectors, La Biodola, Isola d'Elba, Italy, 25–31 May, 1997, Nucl. Instr. and Meth. A 409 (1998) 1–5.
[6] H. Genz, Nucl. Instr. and Meth. 112 (1973) 83.
[7] S. Ramo, Proc. IRE 27 (1939) 584.
[8] E. Gatti et al., Nucl. Instr. and Meth. 193 (1982) 651.
[9] M. Abbrescia et al., Nucl. Instr. and Meth. A 398 (1997) 173.
[10] M. Abbrescia et al., Nucl. Instr. and Meth. A 392 (1997) 155.
[11] E. Cerron Zeballos et al., Nucl. Instr. and Meth. A 396 (1997) 93.
[12] M. Abbrescia et al., Talk given at the CMS Muon group, CERN, March 16, 1997.
[13] P. Camarri et al., Contribution to the IV Workshop on Resistive Plate Chambers and related detectors, 15–16 Oct. 1997, Naples, Italy, Scientifica Acta XIII (2) (1998) 125.
[14] A. Di Ciaccio et al., Contribution to the IV Workshop on Resistive Plate Chambers and related detectors, 15–16 Oct. 1997, Naples, Italy, Scientifica Acta XIII (2) (1998) 179.
[15] ATLAS Technical Design Report, CERN/LHCC/97-22.
[16] A. Lorusso, Thesis, Department of Physics of the University of Bari, 1998, Unpublished.
[17] P. Fonte, Scientifica Acta XI-1 (1996) 359.
[18] A.N. Shiryaev, Probability, Springer, Berlin, 1984, ch. 8, p. 237.